Monthly Notices
of the
ROYAL ASTRONOMICAL SOCIETY

Mon. Not. R. Astron. Soc. **426,** 2283–2290 (2012) doi:10.1111/j.1365-2966.2012.21832.x

Investigation of CTA 1 using a *Suzaku* observation

Lupin C. C. Lin,[1,2⋆] Jumpei Takata,[3] Albert K. H. Kong,[4,8] C. Y. Hui,[5] Teruaki Enoto,[6] H. K. Chang,[4] Regina H. H. Huang,[4] J. S. Liang,[4] Shinpei Shibata[7] and C. Y. Hwang[2]

[1]*General Education Center, China Medical University, Taichung 40402, Taiwan*
[2]*Graduate Institute of Astronomy, National Central University, Jhongli 32001, Taiwan*
[3]*Department of Physics, University of Hong Kong, Hong Kong, China*
[4]*Institute of Astronomy and Department of Physics, National Tsing Hua University, Hsinchu 30013, Taiwan*
[5]*Department of Astronomy and Space Science, Chungnam National University, Daejeon, South Korea*
[6]*Cosmic Radiation Laboratory, Institute of Physical and Chemical Research, 2-1 Hirosawa, Wako, Saitama 351-0198, Japan*
[7]*Department of Physics, Yamagata University, Yamagata 990-8560, Japan*
[8]*Golden Jade Fellow of Kenda Foundation, Taiwan*

Accepted 2012 July 30. Received 2012 July 30; in original form 2012 March 22

ABSTRACT

We report on a 105-ks *Suzaku* observation (obsid 404011010 with J. Takata as PI) of the supernova remnant CTA 1 (G119.5+10.2). The *Suzaku* soft X-ray observation was carried out using both the timing and imaging modes. A ∼10-arcmin extended feature, which is interpreted as a bow-shock component of the pulsar wind nebula, is revealed in this deep observation for the first time. The nebular spectrum can be modelled by a power law with a photon index of ∼1.8, which suggests a slow synchrotron cooling scenario. The photon index is approximately constant across this extended feature. We compare our observations of this complex nebula with previous X-ray investigations, and we discuss our findings. We do not obtain any significant pulsation from the central pulsar in the soft (0.2–12 keV) and hard (10–60 keV) X-ray data. The non-detection is mainly a result of the loss of the precise imaging ability to accurately determine the source contribution. The spectra from the X-ray imaging spectrometer and the hard X-ray detector can be directly connected without a significant spectral break, according to our analysis. Future observations by the *Nuclear Spectroscopic Telescope Array* (*NuSTAR*) and *Astro-H* might be able to resolve the contamination and provide an accurate hard X-ray measurement of CTA 1.

Key words: time – pulsars: general – stars: winds, outflows – ISM: individual objects: CTA 1 (G119.5+10.2) – ISM: supernova remnants – X-rays: general.

1 INTRODUCTION

CTA 1 (G119.5+10.2) is a composite supernova remnant (SNR) with centrally bright X-ray emission (Seward, Schmidt & Slane 1995; Slane et al. 1997). This SNR has a radio shell with a radius of ∼54 arcmin and its kinematic distance, which is estimated from the associated H I emission, is 1.4 ± 0.3 kpc (Pineault et al. 1993). The X-rays from CTA 1 comprise both thermal and non-thermal emission (Seward et al. 1995). While the outer regions mainly consist of shock-heated thermal emission, the non-thermal component dominates the central emission. This has led to the speculation that there is a hidden pulsar in this SNR (Slane et al. 1997). In addition to the radio and X-ray observations, the launch of the *Compton Gamma-Ray Observatory* (*CGRO*) has provided further insight into the nature of CTA 1. The Energetic Gamma Ray Experiment Telescope (EGRET) onboard *CGRO* has revealed a γ-ray source, 2EG J0008+7307 (Thompson et al. 1995), in the second EGRET catalogue (or 3EG J0010+7309 in the third EGRET catalogue; Hartman et al. 1999). It has been suggested that this is associated with CTA 1, because of the positional coincidence (Brazier et al. 1998). The lack of variability of this extended γ-ray source and its spectral resemblance to a typical γ-ray pulsar have further suggested that a neutron star should reside in this SNR. Nevertheless, the limited photon statistics obtained by EGRET have not allowed for any meaningful pulsation search in the MeV–GeV regime.

Observations with *ROSAT* have revealed an X-ray point source, RX J0007.0+7302, at the centre of CTA 1 (Seward et al. 1995). This has also been identified as the X-ray counterpart of 2EG J0008+7307/3EG J0010+7309 (Brazier et al. 1998). This point source has been identified as a neutron star candidate with high γ-ray-to-X-ray and X-ray-to-optical flux ratios as well as its X-ray spectral behaviour (Slane et al. 1997), which was found to be similar to that of the only radio-quiet γ-ray pulsar known at that time – Geminga (Brazier et al. 1998; Halpern et al. 2004). Utilizing the high-resolution imaging capability of *Chandra*, Halpern et al.

⋆E-mail: lupin@crab0.astr.nthu.edu.tw

(2004) have uncovered a torus+jet feature, which resembles the morphology of a pulsar wind nebula (PWN), as seen in other bright γ-ray pulsars. Furthermore, the subarcsec angular resolution of the *Chandra* image has provided a precise position, which can facilitate multiwavelength investigations. To identify the neutron-star nature unambiguously, several attempts have been made to search for the spin period of RX J0007.0+7302 (Biggs & Lyne 1996; Nice & Sayer 1997; Slane et al. 2004; Halpern et al. 2004; Lin & Chang 2005) in different energy bands. Nevertheless, conclusive evidence for pulsations in radio/X-ray has not yet been found in these studies.

With the unprecedented sensitivity of the Large Area Telescope (LAT) onboard the *Fermi Gamma-Ray Space Telescope*, a γ-ray pulsar, LAT PSR J0007+7303, was eventually detected in CTA 1 (Abdo et al. 2008). This source has a spin period of ∼315.86 ms and it was the first radio-quiet γ-ray pulsar detected by the LAT. Its spin parameters imply a characteristic age of ∼14 000 yr, which is consistent with the kinematic age of CTA 1 (∼10 000–20 000 yr; Slane et al. 1997). This strongly suggests an intrinsic association between the pulsar and the SNR. With the discoveries of more radio-quiet γ-ray pulsars (Abdo et al. 2009; Saz Parkinson et al. 2010), we can now examine these as a unique class. It has been speculated that the main distinction between radio-quiet and radio-loud γ-ray pulsars is simply a geometrical effect. In order to further investigate their emitting properties, X-ray observations are required.

Although the periodic signals of these γ-ray pulsars can be detected easily, Geminga is the only radio-quiet γ-ray pulsar whose X-ray pulsation was detected before 2009 (Halpern & Holt 1992). In order to investigate the possible origin of the pulsed X-rays from radio-quiet γ-ray pulsars as a whole class, the search for possible pulsations from these pulsars has been conducted using dedicated X-ray observations, including observations of PSR J0007+7303. Using a ∼120-ks observation from *XMM–Newton* (hereafter *XMM*), the X-ray pulsation of PSR J0007+7303 has been independently detected by Lin et al. (2010) and Caraveo et al. (2010). Apart from the X-ray pulsation, this deep *XMM* observation also reveals the nebular emission extending ∼2 arcmin in the south-east direction away from the pulsar (see fig. 1 of Caraveo et al. 2010). Together with the torus+jet feature found by Halpern et al. (2004), all previous X-ray investigations suggest that LAT PSR J0007+7303 has a complex PWN structure. To continue the investigation, we have observed this interesting object with *Suzaku*, which enables a detailed analysis in both soft and hard X-ray bands. In this paper, we report on the results obtained from analysing the *Suzaku* data.

2 OBSERVATIONS

Suzaku (Mitsuda et al. 2007) was built with two main payloads, five nested conical thin-foil grazing incidence telescopes (XRT; Serlemitsos et al. 2007) with the effective energy range of 0.2–12 keV and a hard X-ray detector (HXD; Takahashi et al. 2007) with the effective energy range of 10–600 keV. There are two major detectors for spectroscopy – the X-ray spectrometer and the X-ray imaging spectrometer (XIS) – in *Suzaku*, and each of these is set at the focus of an XRT. Our observational results on the temporal and spectral analyses mainly come from the XIS (Koyama et al. 2007) and the HXD. The XIS consists of three front-illuminated (FI; XIS0, XIS2, XIS3) and one back-illuminated (BI; XIS1) CCD detectors, but only the FI chips provide the observations in the timing/P-SUM mode. Because the time resolution of the HXD is 61 μs and that of XIS in the timing mode is ∼7.8 ms, our data are precise enough for the periodicity search for a radio-quiet γ-ray pulsar with a spin period of tens or hundreds of milliseconds. However, two of the XIS units with FI chips, XIS0 and XIS2, suffered catastrophic damage in 2006 November and 2009 June, respectively. Because no useful data can be obtained with XIS2 and part of the segment in XIS0 has been lost, only the observations from the XIS3 unit can be used for temporal analysis. These events have seriously decreased the probability that periodic signals can be obtained from faint sources in the soft X-ray band. There are also two independent detector systems used for the observations of the HXD. The positive-intrinsic-negative (PIN) silicon diodes are sensitive below ∼60 keV in the field of view (FOV) of 34 × 34 arcmin^2, and the gadolinium silicate/bismuth germanate crystal (GSO/BGO) phoswich counters can detect photons above ∼30 keV in the FOV of $4.^\circ5 \times 4.^\circ5$. Because the data obtained from the HXD have no imaging capability, we only carried out an analysis of the HXD–PIN data, in order to avoid the contamination caused by the large background size of the HXD–GSO, which is much larger than the size of CTA 1.

Our observation for CTA 1 was carried out on 2010 January 8 with total exposures of ∼105 ks in the soft X-ray band and ∼59 ks in the hard X-ray band. It was aimed at the HXD nominal position to RX J0007.0+7302 with (J2000) RA = $00^{\rm h}07^{\rm m}02\overset{\rm s}{.}2$, Dec. = $+73^\circ03'07''$ (Slane et al. 2004). The XIS0 and XIS1 data of *Suzaku* were observed in the normal mode without the window option, while the *Suzaku*/XIS3 data observed within 128 rows were compressed into one dimension to attain a higher time resolution. All the data reduction and the spectral analyses were performed using XSELECT (version 2.4a), FTOOLS (version 6.9) and XSPEC (version 12.6.0) of HEASOFT (version 6.9) with the latest *Suzaku*/XIS calibration files (20101108) and *Suzaku*/HXD calibration files (20101202).

2.1 XIS0 and XIS1

The XIS0 and XIS1 observations of the 105-ks exposures were divided into two editing modes of 3 × 3 and 5 × 5 with ∼85 and ∼20 ks, respectively. Because each pixel on the CCD was read out every 8 s in the normal mode, the time resolution of the XIS0 and XIS1 data is not accurate enough to search for the periodic signal in a range of less than 1 s. However, the XIS0 and XIS1 data are still adequate for the spectral analyses of the X-ray point source and the PWN in order to compare with the results yielded by other X-ray missions. The adoption for the centre of the point source is referred to as the aim point of the *Suzaku* observation. Because RX J0007.0+7302 is seriously contaminated by the surrounding PWN, we have extracted the spectra of RX J0007.0+7302 only within a 1.5-arcmin central circular region instead of the regular choice of 3-arcmin circular region for a point source. This option still contains ∼75 per cent of the encircled energy fraction (EEF). We have extracted the background of the pulsar from a concentric annulus of radii $100 < r \leq 180$ arcsec, centred at the aim point of this *Suzaku* observation. The spectra extracted from the point source comprise 695 counts for XIS0 and 401 counts for XIS1, after subtracting the background. We have also considered the point-source selection in two other different sizes with 2 and 3 arcmin in radii using the same centre, as shown in Table 1. These selections of the point source contain ∼85 and ∼95 per cent of the EEF, respectively. The backgrounds of these selected regions were determined within a concentric annulus of radii $2 < r \leq 4$ arcmin and $3 < r \leq 4.5$ arcmin, respectively. Different choices for a point-source region are used to verify that the significant excess contributed by the surrounding PWN can be detected with the increasing size.

For the PWN, first we examined its source extent by applying adaptive smoothing to both XIS0 and XIS1 images. The images

Table 1. Best-fitting parameters for the spectral fits to the pulsar in CTA 1 using *Suzaku*/XIS0 and XIS1 observations. Small, medium and large indicate the source selection with different sizes. The small, medium and large point-source regions were adopted with the same centre and circles with 1.5, 2 and 3 arcmin in radii, which correspond to the EEF of ∼75, 85 and 95 per cent. The background contributions were determined within a concentric annulus of radii $100 < r \leq 180$, $120 < r \leq 240$ and $180 < r \leq 270$ arcsec, respectively.

	RX J0007.0+7302/PL		
Parameter	Small	Medium	Large
$N_{\rm H}$ (cm^{-2}; fixed)	2.8×10^{21}	2.8×10^{21}	2.8×10^{21}
Γ	$1.76^{+0.27}_{-0.25}$	1.80 ± 0.15	$1.85^{+0.14}_{-0.12}$
$F_{\chi,\rm PL} \times 10^{-13}$ (erg cm^{-2} s^{-1})[a]	3.7 ± 1.1	4.6 ± 1.0	7.1 ± 1.3
χ^2/d.o.f.	39.0/46	78.2/85	157.4/143

[a] The unabsorbed flux is measured in the energy range of 0.3–10 keV.

shown in Fig. 1 were generated taking into account the vignetting of the XRT. We used the task 'xissim' to simulate a flat-field image for our purpose, and we have displayed the obtained image after dividing by the flat field. A large structure with an extent of ∼10 arcmin appears to extend eastward from the pulsar. In view of the possible spectral steepening as a result of synchrotron cooling, we performed a spatially resolved spectral analysis of the PWN. The extraction regions are illustrated in Fig. 2. We split the PWN into three regions: the inner part (a circular region within a radius of 2 arcmin), the middle part (an annulus with radii $2 < r < 4$ arcmin) and the outer part (a panda region with radii $4 < r < 8$ arcmin). The background spectra are sampled from the source-free low-count regions from each detector, respectively. We only consider the spectra obtained with the 3×3 mode to perform the spectral analysis of the

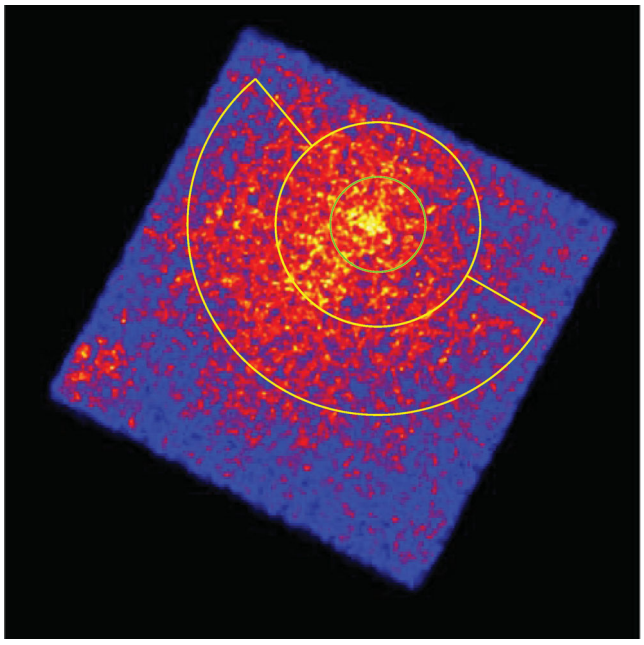

Figure 2. Illustration of the regions used to extract the spectra from different parts of the PWN associated with RX J0007.0+7302.

PWN, because of its better photon statistics. To yield better photon statistics for describing the spectral behaviour for the PWN, we have rebinned all the spectra before the analysis. We generated the spectrum with >200 counts per bin for the inner part, and with >500 counts per bin for the middle and outer parts.

We generated the associated response matrix (rmf) and auxiliary response (arf) files using the HEASOFT command of XISRMFGEN and XISSIMARFGEN. The spectrum obtained from each detector was rebinned with a minimum of 30 counts per channel to ensure χ^2

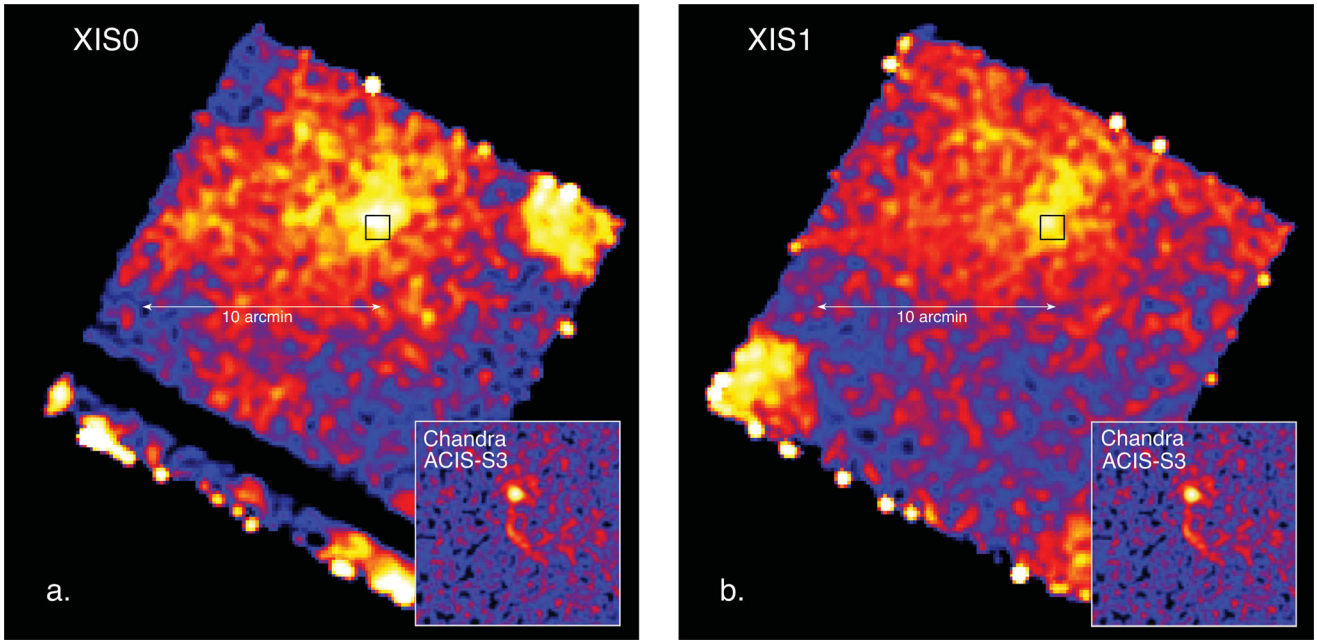

Figure 1. Vignetting-corrected images of the field around RX J0007.0+7302 as observed by *Suzaku*/XIS0 (a) and *Suzaku*/XIS1 (b). A PWN component with an extent of ∼10 arcmin is revealed. The lost of the row image shown in *Suzaku*/XIS0 (a) was supposed to be caused by an event of the micrometeorite hit. The inset shows the close-up view of the 1×1 arcmin^2 region (illustrated by the black square) around the pulsar, as seen by *Chandra* (adopted from Halpern et al. 2004). For both images, top is north and left is east.

statistics. Then, we introduced a constant in a simultaneous fit to account for the cross-calibration mismatch between different detectors. We have also considered different circular sizes to describe the contribution of the point source. Details about the spectral results are presented in Section 3.

2.2 XIS3

The XIS3 data were investigated using the timing/P-SUM mode with a long duration of ∼212 ks, and the image has been compressed into one dimension without the information along the *Y*-axis, in order to obtain a higher time resolution. Our procedures to resolve the point source in a one-dimensional image follow the standard recipe for reducing XIS data with the timing mode (Matsuta et al. 2010). We have also redone the event reprocessing to consider the grade filtering and we have generated the new cleaned event file using the script XISREPRO.XCO with the proper selection criteria. For the P-SUM mode, we need to remove the hot pixels on the image manually. To identify these hot pixels, we accumulated all the photon events along the coordinate of ACTX. First, we removed the columns that had significantly more photons than others. Then, we counted the distribution of events in the remaining columns and removed those pixels with photons exceeding 3σ more than the median of the distribution.

After excluding all the hot pixels, the source was still too marginal to be resolved in the histogram of ACTX versus photon events of the XIS3 data. Thus, we tried to rebin the distribution of counts along ACTX with several pixels, as shown in Fig. 3. A point-like source with 112 pixels (∼118 arcsec) can be roughly detected close to the centre when we rebin with 32 pixels. There are 58 255 photons for this source within 0.2–12 keV and the significance of this detection is $\sim 3.3\sigma$. We have also checked the absolute arrival time of the photon events and we have determined the time required for readout by the ACTX position of the source in the XIS1 image. In order to perform a precise temporal analysis, we have corrected the arrival time with a decrease of 31.2 ms for all the source photons. The Solar system barycentric time correction was then implemented with the task AEBARYCEN at (J2000) RA = $00^{\rm h}07^{\rm m}01\overset{\rm s}{.}56$, Dec. = $+73^\circ03'08\overset{''}{.}1$ (Halpern et al. 2004) to yield a time list that can be used to examine

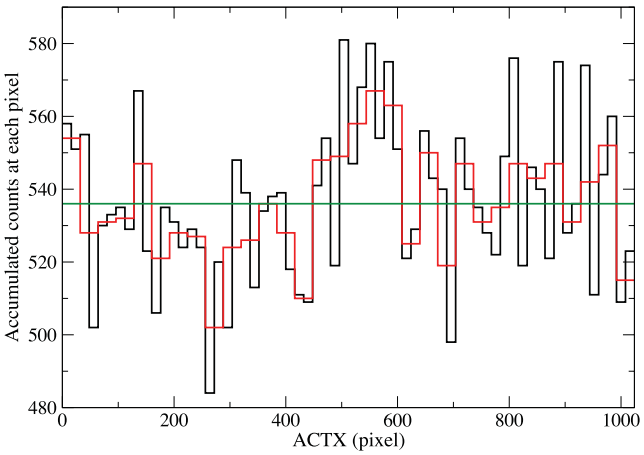

Figure 3. Histogram of ACTX versus photon distribution of the XIS3 data. The black solid line marks the average photons of each pixel after rebinning the ACTX with 16 pixels, and the red line shows the distribution with the bin of 32 pixels. The green solid line is set as 536 to demonstrate the median of the photon distribution. A point-like source can marginally be resolved within the range of the 496–608 pixels in the red line.

the pulsation of RX J0007.0+7302/PSR J0007+7303 in the soft X-ray band.

2.3 HXD

The HXD observation was conducted in nominal pointing. Because the HXD is a non-imaging instrument, we cannot separate the contribution of the pulsar from the surrounding nebula. However, a spectrum can be acquired to describe the behaviour of the total hard X-rays emitted from the entire CTA 1.

We only focus on the HXD–PIN detections of the hard X-rays emitted from/around CTA 1. In order to examine the periodic signal of the pulsar, we have also applied the Solar system barycentric time correction with the task AEBARYCEN at (J2000) RA = $00^{\rm h}07^{\rm m}01\overset{\rm s}{.}56$, Dec. = $+73^\circ03'08\overset{''}{.}1$ (Halpern et al. 2004) on the HXD–PIN observation. The events in the observation were restricted according to the effective energy range (10–60 keV) of the PIN detector, and 26 661 photons were obtained for temporal analysis after the screening of the energy.

We have also subtracted the non-X-ray background (NXB) and cosmic X-ray background (CXB) to obtain the HXD–PIN spectrum. The simulated NXB was directly obtained from the *Suzaku* Data Center, and the CXB flux (i.e. ∼5 per cent of the NXB for PIN) can be derived from (Boldt 1987)

$$CXB(E) = 9.412 \times 10^{-3} (E/1\,\mathrm{keV})^{-1.29} \exp(-E/40\,\mathrm{keV}) \quad \mathrm{photons\ cm^{-2}\ s^{-1}\ FOV^{-1}\ keV^{-1}}. \tag{1}$$

These background spectra correspond to epoch '6' for the flat PIN response matrix. We have also evaluated the contribution of the Galactic Ridge X-ray Emission (GRXE) using the *Suzaku* observation of a nearby blank sky (OBSID = 504039010) at $(l, b) = (123\overset{\circ}{.}9, 10\overset{\circ}{.}0)$, which is $4\overset{\circ}{.}3$ from CTA 1. Following the same method as in Enoto et al. (2010), we have assumed a power-law spectrum with a fixed photon index at 2.1 (Valinia & Marshall 1998). The contribution of the GRXE within 14–35 keV was evaluated to be $<4.4 \times 10^{-4}$ photons $\mathrm{s^{-1}}$, which only corresponds to <0.2 per cent of the NXB. Thus, the contribution of the GRXE is negligible when we analyse the HXD–PIN spectrum of CTA 1. After the background subtraction, we rebinned the spectrum to ensure that the photon numbers in each channel were larger than 30.

3 RESULTS

3.1 Timing analysis

The expected spin frequency of the pulsar in our *Suzaku* data can be inferred from the contemporaneous *Fermi* ephemeris (Ray et al. 2011). The start of GTI for our *Suzaku*/XIS3 and HXD–PIN data is at epoch MJD 55204.6143077. The spin frequency of PSR J0007+7303 corresponding to this epoch can be inferred as 3.165750271(6) $\mathrm{s^{-1}}$ with the first frequency derivative of $-3.6136(2) \times 10^{-12}$ $\mathrm{s^{-2}}$ (the effect of the second frequency derivative is negligible). We have searched for periodic signals with the known first frequency derivative around the predicted frequency in *Suzaku*/XIS3 and HXD–PIN data using the *H*-test (de Jager, Raubenheimer & Swanepoel 1989). The *H*-value is only 11.7, corresponding to the expected spin frequency of 3.165750271(6) $\mathrm{s^{-1}}$ for the *Suzaku*/XIS3 observation, and only 6.7 for the *Suzaku*/HXD–PIN observation. Fig. 4 demonstrates the periodicity search of 200 independent trials around the expected spin frequency of PSR J0007+7303. We conclude that no significant pulsed detection can

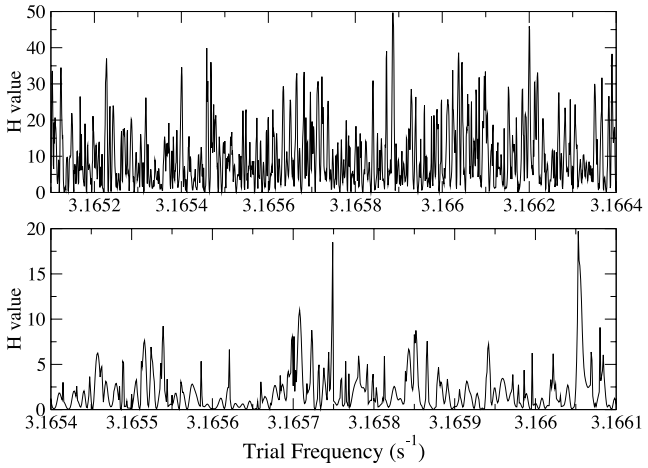

Figure 4. Periodicity search of the *Suzaku* data using the H-test. Each panel presents the search with 200 independent trials close to the expected spin frequency of PSR J0007+7303 at the observational epoch. The upper panel shows the search results of the *Suzaku*/XIS3 data, and the width of each independent trial is $\sim 4.7 \times 10^{-6}$ s^{-1}. The lower panel shows the search results of the *Suzaku*/HXD–PIN data, and the width of each independent trial is $\sim 6.0 \times 10^{-6}$ s^{-1}.

be yielded from our *Suzaku* data, in both the soft and hard X-ray bands.

Compared with the soft X-ray pulsation detected by the *XMM* observation (Lin et al. 2010; Caraveo et al. 2010), our *Suzaku* data lose one-dimensional imaging ability in the XIS3 timing mode, and we have no imaging ability in the *Suzaku*/HXD investigation. In the *Suzaku*/XIS3, we can only have a marginal detection to resolve the point source with ∼58 000 photons, as shown in Section 2.2. However, the counts gathered in the source region are much more than we expected, based on the spectral behaviour provided by Slane et al. (1997). We note that most of the additional counts obtained from the P-SUM mode data are caused by the instrumental background. For the data detected in the hard X-ray band, the main contribution of the hard X-ray photons is ascribed to the X-ray background. If we assume the pulsed spectrum of Caraveo et al. (2010), the expected signal-to-noise ratio of the *Suzaku* investigation is too low ($<2\sigma$) to yield the periodic signal from the pulsar.

We have also examined this spin frequency using the ∼three-month *Fermi* archive (2009 November 22 to 2010 February 21) on the epochs close to our *Suzaku* observation. The effective γ-ray photons of PSR J0007+7303 were restricted in a 1-deg circle centred at (J2000) RA = 1.°7565, Dec. = +73.°05225 (Halpern et al. 2004) within the energy range from 100 MeV to 300 GeV. We determined the spin frequency of the pulsar with the H-test using the task GTPSEARCH from the *Fermi* Science Tools (version v9r15p2). At epoch MJD 55204.6143077, the maximum statistic was obtained at 3.16575026(1) s^{-1} with the first frequency derivative of $-3.6136(2) \times 10^{-12}$ s^{-2}. This result is consistent with the aforementioned prediction.

3.2 Spectral analysis

We have derived the soft X-ray spectrum from XIS0 and XIS1 onboard *Suzaku*. Based on our selected region for the X-ray point source, the ratio of net source counts for the pulsar to the total photons in the source region considered in the spectrum of XIS0 is more than 25 per cent, but in that of XIS1 it is only ∼10 per cent. This is because the BI chip (XIS1) has a higher effective area at low energies. We have only considered the spectral fits in the range 0.5–10 keV and we have ignored photons outside this energy range to avoid large uncertainties. A cross-calibration term was included to correct for the difference among the XIS spectra, and the result is consistent with the fit to the spectrum of any individual detector. The absorption was fixed at 2.8×10^{21} cm^{-2} according to previous measurements (Slane et al. 1997; Lin et al. 2010), which is consistent with optical extinction (Halpern et al. 2004). A single power law provides an acceptable fit, as shown in Table 1 and Fig. 5. Our data are not good enough to give a good constraint for an additional model component, such as a thermal blackbody model or a magnetized neutron star atmosphere (NSA; Zavlin, Pavlov & Shibanov 1996) model. However, we note that the source fluxes derived from different sizes seem to be larger than those of previous studies and they increase with source sizes; these excesses might be a contribution from the PWN.

However, our deep *Suzaku* observation provides a good opportunity to investigate the PWN, particularly for faint emission extending to ∼10 arcmin (see Fig. 1). Previous observations with *Chandra* (Halpern et al. 2004) and *XMM* (Caraveo et al. 2010) failed to detect this large but faint diffuse structure. This was probably because of the relatively small collecting area of *Chandra* and the high instrumental background of *XMM*.

In order to properly constrain the non-thermal X-ray contributions from the PWN, we have also fixed the column density at $N_{\rm H} = 2.8 \times 10^{21}$ cm^{-2}. Besides a power-law model for PWN emission, we have also included an additional power-law component to account for X-rays from the pulsar, with the parameters fixed at those inferred by Caraveo et al. (2010). For each of the three regions that we consider, we have scaled the spectral component of the pulsar with the EEF or the contribution from the wing of the point spread function (PSF) centred at the pulsar, accordingly, by multiplying a constant. The best-fitting parameters of the power-law component of the PWN inferred from the spatially resolved spectral analysis are summarized in Table 2. Taking the statistical uncertainties into consideration, no evidence for spectral steepening can be found from this observation. The whole diffuse X-ray feature can be modelled using a power law with a photon index of $\Gamma \sim 1.8$.

We have also derived the hard X-ray spectrum from the HXD–PIN. After subtracting the background, the net counts of the hard X-rays collected for the spectrum are only 6.6 per cent in total. Because there are abnormal accumulations for photons at both limits of the effective energy boundary in our HXD–PIN observation, we only consider the hard X-ray spectrum within the energy range of 14–30 keV. Fig. 6 shows the spectrum fitted to a power-law model with the photon index (Γ) of 3.0. We have also checked the systematic uncertainty of the background from other observations, and the NXB accuracy should be within a 5 per cent level in the range of 15–40 keV around the CTA 1 observation. The nominal uncertainty of the adopted background model is also indicated in Fig. 6. Because the effective data points of our hard X-ray spectrum are few, the uncertainty is very large and the best fit cannot be determined well. We have fixed the absorption as 2.8×10^{-21} cm^{-2}, according to the column density obtained by Slane et al. (1997). A photon index of $\Gamma = 3.33^{+2.18}_{-1.81}$ (90 per cent confidence level) with $\chi^2_\nu = 1.15$ for 10 d.o.f. can be yielded in the investigation of our hard X-ray spectrum. Taking into account the wide spread of the acceptable photon index, the total unabsorbed flux in the range of 10–50 keV for the whole FOV of the HXD–PIN inferred from these acceptable fits is distributed from $\sim 7.8 \times 10^{-12}$ to $\sim 1.1 \times 10^{-11}$ erg cm^{-2} s^{-1}, and this signal remains between the ∼3 and 5 per cent level of the NXB at the 90 per cent confidence level. The hard

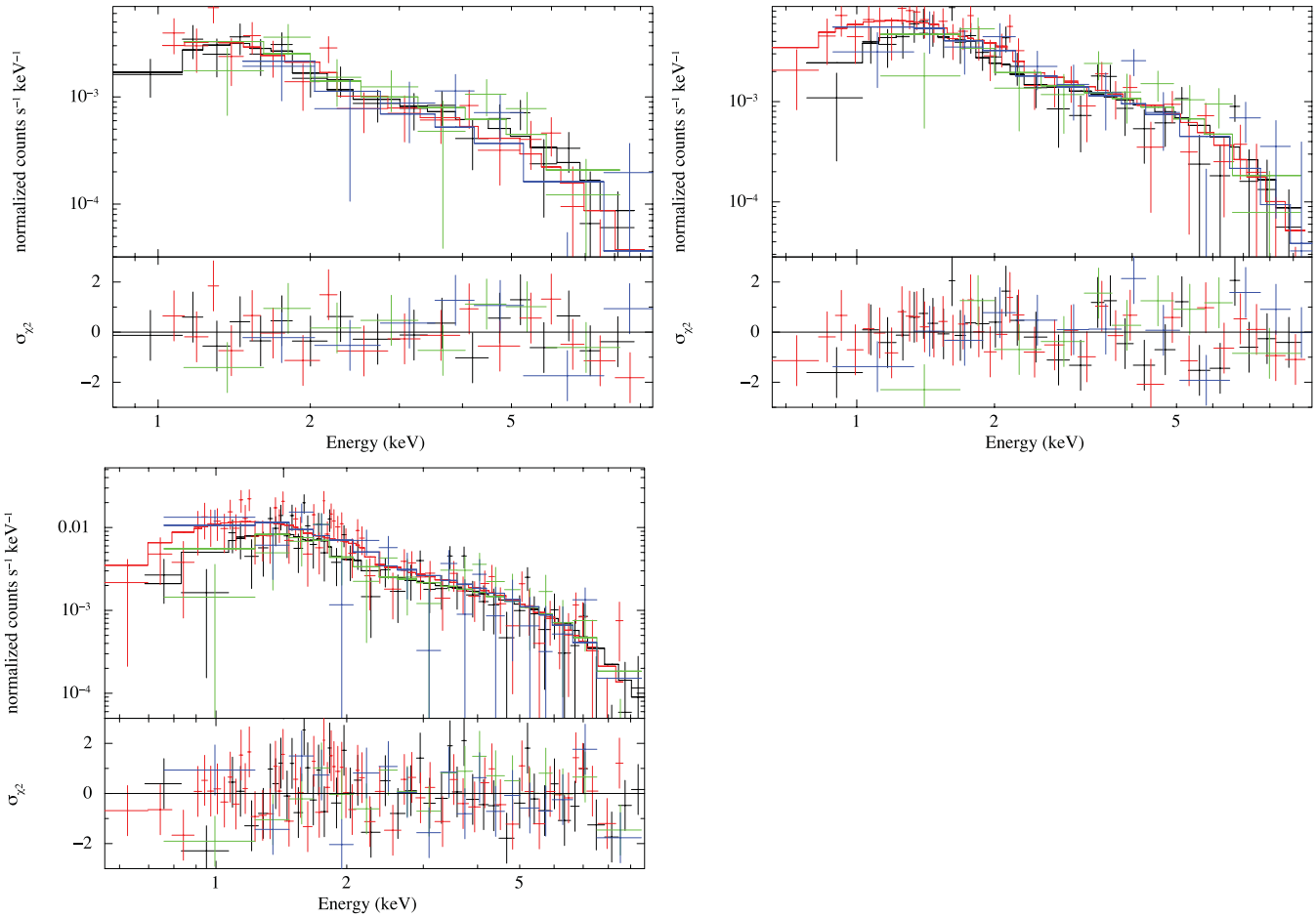

Figure 5. Spectral fits to the power-law model. The first row presents the spectral fits to the point source centred in CTA 1 with selected circles of 1.5 and 2 arcmin in radii, respectively. The second row presents the spectral fit to the point source centred in CTA 1 with a selected circle of 3 arcmin. The black and green data sets refer to the XIS0 observations of 3 × 3 and 5 × 5 modes, respectively, while the red and blue data sets refer to the XIS1 observations of 3 × 3 and 5 × 5 modes respectively. The detailed parameters of these fits are shown in Table 1.

Table 2. Best-fitting parameters of the power-law spectral components inferred from different regions of the PWN around PSR J0007+7303. The column density is fixed at $N_{\rm H} = 2.8 \times 10^{21}$ cm^{-2} for all these spectral fits. An additional power-law component to account for the pulsar emission, with the parameters fixed at those inferred by Caraveo et al. (2010) (i.e. $\Gamma = 1.36$ with $f_{\rm PSR} = 6.5 \times 10^{-14}$ erg cm^{-2} s^{-1}), is included with a multiplicative factor for scaling the pulsar contributions in each region accordingly (i.e. 85, 10 and 5 per cent for inner, middle and outer parts, respectively.

Region	Γ	$f_{\rm pwn}$ (0.3–10 keV) erg cm^{-2} s^{-1}	χ^2/d.o.f.
Inner part	1.89 ± 0.08	$1.2^{+0.2}_{-0.1} \times 10^{-12}$	30.0/28
Middle part	1.79 ± 0.09	$(1.4 \pm 0.2) \times 10^{-11}$	38.1/34
Outer part	1.92 ± 0.11	$1.5^{+0.3}_{-0.2} \times 10^{-11}$	38.4/41

X-rays detected in the region around CTA 1 are also consistent with a previous *INTEGRAL* investigation (Sturner et al. 2004).

4 DISCUSSION

We have investigated the central region of CTA 1 using a deep *Suzaku* observation. For the X-ray flux of RX J0007.0+7302, as

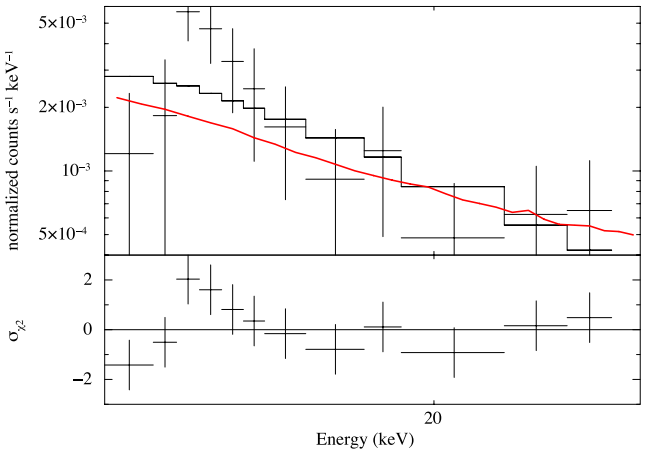

Figure 6. Spectral fit to the *Suzaku*/HXD–PIN observation in 14–30 keV. The solid line represents the best fit to a single power law with the photon index of 3.0, and corresponds to the unabsorbed flux of ∼8.0 × 10^{-12} erg cm^{-2} s^{-1} in the range of 10–50 keV. The red line demonstrates the systematic errors that correspond to ∼5 per cent of the NXB distribution. The bottom panel shows the residuals in terms of σ.

estimated by the XIS data, we note that it is larger than that reported by Lin et al. (2010) and Caraveo et al. (2010) using an *XMM* observation. This discrepancy could be because the PSF of *Suzaku* is considerably wider than that of *XMM*. In view of this, the contribution of the point source is likely to be contaminated by the surrounding PWN. This is the main reason why we cannot obtain the real spectrum of the pulsar. Because of the loss of the imaging ability in the *Suzaku* data for the periodicity examination, we cannot separate the instrumental effect in the soft X-ray band and the serious contamination from the X-ray background in the hard X-ray band. These problems prevent the pulsed detection from the current *Suzaku* observation. Because the *Suzaku* data do not provide a constrained result for the timing properties of RX J0007.0+7302/PSR J0007+7303, we cannot obtain the phase-resolved spectroscopy and we do not discuss the nature of this point source any further in the following.

We have also examined the properties of the PWN with the XIS data. A single power law can provide a good fit, and we have not detected any additional thermal X-rays emitted in the central region of CTA 1, which is consistent with previous investigations (e.g. Slane et al. 1997). Both the flux and the photon index obtained in our independent investigation are fully consistent with those inferred by the recent *XMM* observation (Caraveo et al. 2010).

We would like to discuss the possible nature of the nebula that extends eastward, as discovered by our deep *Suzaku* exposure. The feature revealed by *Suzaku* extends as much as ∼10 arcmin, while the *XMM* observations only detected an nebular feature with an extent of a few arcmin, which might correspond to the relative brighter component of the nebula (see fig. 1 of Caraveo et al. 2010). The spectral steepness and the flux of the inner part in our investigation are consistent with their results (refer to 'Outer PWN' in table 1 of Caraveo et al. 2010). The morphology of this extended feature appears to be asymmetric (see Fig. 1), which resembles those of bow-shock nebulae, such as PSR J1747–2958 (Gaensler et al. 2004). Such extended features are usually along the direction of pulsar motion and behind the bow-shock, and therefore they are interpreted as the synchrotron radiation from the flow of particles coming out of the PWNe.

It is instructive to discuss the plausible relation between this large feature and the torus+jet of a smaller scale reported in fig. 1 of Halpern et al. (2004); this is also shown in the inset of our Fig. 1. The *Chandra* image shows that the jet has an extent of ∼16 arcsec towards the south and bends to the south-west at the far end from the pulsar (see Fig. 1). However, the compact torus-like feature with a radius of ∼3 arcsec around the pulsar appears to be elongated in a direction perpendicular to the jet. Halpern et al. (2004) have interpreted this system as an equatorial torus with the jet emitted along the rotation axis, and this is observed in many PWN systems (for a review, see Ng & Romani 2004).

If the ∼10-arcmin feature is indeed a result of the bow-shock, as mentioned previously, this suggests that the pulsar is possibly moving west. This speculated pulsar motion is almost perpendicular to the portion of the jet close to the pulsar (see Fig. 1). The origin of the velocity of pulsars is still an open question. One possible mechanism is the asymmetric supernova explosion. Apart from giving rise to the kick velocity, this also contributes to the initial spin of a pulsar (Spruit & Phinney 1998; Lai, Chernoff & Cordes 2001). If the initial spin angular momentum of RX J0007.0+7302 is dominated by the kick process, the jet emitted along the rotational axis should be more or less perpendicular to the direction of proper motion, which can explain the relative orientation between the jet and the ∼10-arcmin feature. Therefore, the measurement of the proper motion of RX J0007.0+7302 with multi-epoch X-ray imaging (e.g. Hui & Becker 2006), and/or a dedicated γ-ray pulsar timing solution yielded from LAT data, can help to constrain the relation among the various extended features of this complex system.

Although the exact origin of this large extended feature remains uncertain, the X-ray spectral analysis confirms its non-thermal nature. Assuming it is a synchrotron nebula, we discuss its emission properties in further detail. For the synchrotron-emitting electrons distributed as $N(\gamma) \propto \gamma^{-p}$, where γ is the Lorentz factor of the wind particles, the resultant X-ray photon index Γ depends on whether the emission is in a fast or slow cooling regime (Cheng, Taam & Wang 2004). This is determined by the cooling frequency of the emitting region

$$\nu_c = \frac{18\pi e m_e c}{\sigma_{\rm T}^2 \tau_{\rm syn}^2 B^3},$$

where $m_{\rm e}$, $\sigma_{\rm T}$, $\tau_{\rm syn}$ and B are the electron mass, Thomson cross-section, synchrotron lifetime and magnetic field strength, respectively. We have $\Gamma = (p + 2)/2$ for a fast cooling scenario (i.e. $\nu_x > \nu_c$) and $\Gamma = (p + 1)/2$ for a slow cooling scenario (i.e. $\nu_x < \nu_c$). For a standard shock model, p spans a range of ∼2–3 (see Cheng et al. 2004, and references therein). This implies that Γ should span the ranges of ∼2–2.5 and ∼1.5–2 for the fast cooling and slow cooling scenarios, respectively. Comparing these ranges with the values inferred in the XIS spectrum (see Table 2), we suggest that the inner and middle parts of this PWN are probably in a slow cooling regime. For the outskirts of the nebula, the best-fitting photon index suggests that the synchrotron cooling in this region is also slow. However, within the 90 per cent confidence interval of the inferred photon index, it is on the margin of both regimes. For the inner and middle regions of the PWN, we speculate that ν_c should lie beyond the energy range covered by XIS. Assuming that $h\nu_c \sim 10$ keV and that the synchrotron lifetime of the emitting electrons is comparable with the characteristic age of the pulsar (i.e. $\tau_{\rm syn} \sim 1.4 \times 10^4$ yr), the magnetic field strength in the emitting region can be estimated to be of the order of $B \sim 2$ μG, which is comparable with the typical field strength in the interstellar medium (see Beck et al. 2003, and references therein).

Apart from the observation in the soft X-ray band, we have also investigated the field of CTA 1 with the hard X-ray data collected by HXD–PIN. The spectrum obtained in this hard band (i.e. 14–30 keV) can be described by a power law with $\Gamma = 3.33^{+2.18}_{-1.81}$. The unabsorbed flux in the range of 10–50 keV is found to be $f_x \sim (0.8$–$1.1) \times 10^{-11}$ erg cm^{-2} s^{-1}. We note that the photon index inferred in this band cannot be tightly constrained; however, within the 90 per cent confidence interval, the HXD spectrum can be smoothly connected with the spectrum inferred from the soft band, although it might have slight spectral steepening, as shown in Fig. 7.

We should point out that the true nature of the hard X-ray emission is not yet conclusive. The FOV of the HXD is ∼34 × 34 arcmin^2, while the size of PWN in the soft X-ray is only $\lesssim$10× 10 arcmin^2. In view of the lack of imaging capability of HXD–PIN, the observed hard X-rays can possibly be contributed by other sources in the FOV of *Suzaku*. This might indicate a steeper spectral break than that observed. However, the effects caused by the systematic uncertainty of the NXB background could be large. For example, if the NXB level is lower by a few per cent (e.g. 2 per cent, which is the nominal value of the NXB uncertainty; Fukazawa et al. 2009) than the assumed value, the true hard X-ray would be higher than the current detection and the spectral break would not be as significant as observed. Because there are several upcom-

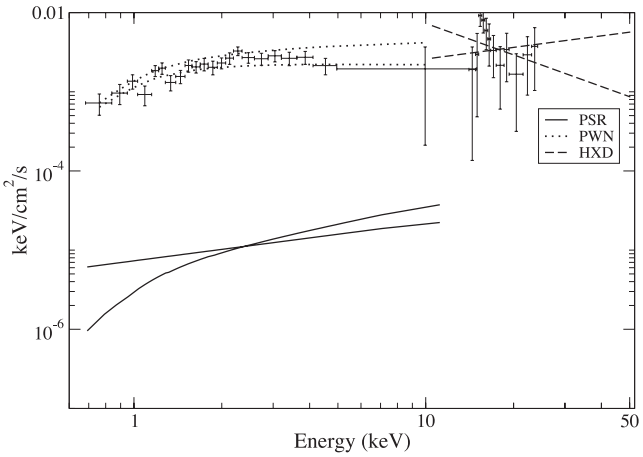

Figure 7. Broad-band absorbed spectrum of PSR J0007+7303, PWN in the soft X-ray band and hard X-ray detection of CTA 1. The absorption in the low-energy band is fixed as 2.8×10^{-21} cm^{-2} following Table 2. The spectral behaviour of the pulsar is determined by the power-law fit from table 1 of Caraveo et al. (2010). The spectrum and the data points for the PWN are derived from the outer region (the data include ∼5 per cent contribution of the pulsar; see Table 2). The solid, dotted and dashed lines represent the uncertainty ranges of the spectral behaviour of the PSR, PWN and HXD, respectively.

ing missions, including the *Nuclear Spectroscopic Telescope Array* (*NuSTAR*; Hailey et al. 2010) and *Astro-H* (Takahashi et al. 2010), which will be capable of imaging the sky up to ∼80 keV for the first time, the exploration of PWNe, including the one in CTA 1, will enter a new era in the near future.

ACKNOWLEDGMENTS

We thank Prof. Yuji Urata in National Central University and Ms. Ting-Ni Lu in National Tsing Hua University of Taiwan for discussions on the examination of the spectra and the vignetting-correction of image for our *Suzaku* observation. This work was partially supported by the National Science Council (NSC) of Taiwan through grants NSC 99-2811-M-008-057 and NSC 101-2112-M-039-001-MY3. RHHH is supported through grants NSC 99-2811-M-007-062 and NSC 100-2811-M-007-040. CY Hwang acknowledges support from the NSC through grants NSC 99-2112-M-008-014-MY3 and NSC 99-2119-M-008-017. AKHK acknowledges support from the NSC through grant NSC 100-2628-M-007-002-MY3. CY Hui is supported by the National Research Foundation of Korea through grant 2011-0023383.

REFERENCES

Abdo A. A. et al., 2008, Sci, 322, 1218
Abdo A. A. et al., 2009, Sci, 325, 840
Beck R., Shukurov A., Sokoloff D., Wielebinski R., 2003, A&A, 411, 99
Biggs J. D., Lyne A. G., 1996, MNRAS, 282, 691
Boldt E., 1987, in Hewitt A., Burbidge G., Fang L. Z., eds, Proc. IAU Symp. 124, Observational Cosmology. Kluwer, Dordrecht, p. 611
Brazier K. T. S., Reimer O., Kanbach G., Carraminana A., 1998, MNRAS, 295, 819
Caraveo P. A., De Luca A., Marelli M., Bignami G. F., Ray P. S., Saz Parkinson P. M., Kanbach G., 2010, ApJ, 725, L6
Cheng K. S., Taam R. E., Wang W., 2004, ApJ, 617, 480
de Jager O. C., Raubenheimer B. C., Swanepoel J. W. H., 1989, A&A, 221, 180
Enoto T. et al., 2010, PASJ, 62, 475
Fukazawa Y. et al., 2009, PASJ, 61, 17
Gaensler B. M., van der Swaluw E., Camilo F., Kaspi V. M., Baganoff F. K., Yusef-Zadeh F., Manchester R. N., 2004, ApJ, 616, 383
Hailey C. J. et al., 2010, Proc. SPIE, 7732, 77320T
Halpern J. P., Holt S. S., 1992, Nat, 357, 222
Halpern J. P., Gotthelf E. V., Camilo F., Helfand D. J., Ransom S. M., 2004, ApJ, 612, 398
Hartman R. C. et al., 1999, ApJS, 123, 79
Hui C. Y., Becker W., 2006, A&A, 457, L33
Koyama K. et al., 2007, PASJ, 59, 23
Lai D., Chernoff D. F., Cordes J. M., 2001, ApJ, 549, 1111
Lin L., Chang H., 2005, Ap&SS, 297, 361
Lin L. C. C., Huang R. H. H., Takata J., Hwang C. Y., Kong A. K. H., Hui C. Y., 2010, ApJ, 725, L1
Matsuta K., Higashi K., Tsujimoto M., The XIS Team, 2010, Recipe for Reducing XIS Data Taken with the P-sum/timing Mode. *Suzaku* Data Center. Available online at http://www.astro.isas.jaxa.jp/suzaku/analysis/xis/
Mitsuda K. et al., 2007, PASJ, 59, 1
Ng C-Y., Romani R. W., 2004, ApJ, 601, 479
Nice D. J., Sayer R. W., 1997, ApJ, 476, 261
Pineault S., Landecker T. L., Madore B., Gaumont-Guay S., 1993, AJ, 105, 1060
Ray P. S. et al., 2011, ApJS, 194, 17
Saz Parkinson P. M. et al., 2010, ApJ, 725, 571
Serlemitsos P. J. et al., 2007, PASJ, 59, 9
Seward F. D., Schmidt B., Slane P., 1995, ApJ, 453, 284
Slane P., Seward F. D., Bandiera R., Torii K., Tsunemi H., 1997, ApJ, 485, 221
Slane P., Zimmerman E. R., Hughes J. P., Seward F. D., Gaensler B. M., Clarke M. J., 2004, ApJ, 601, 1045
Spruit H., Phinney E. S., 1998, Nat, 393, 139
Sturner S. J., Beckmann V., Bykov A., Lebrun F., Terrier R., 2004, in Schoenfelder V., Lichti G., Winkler C., eds, ESA SP-552, Proc. 5th *INTEGRAL* Workshop on the *INTEGRAL* Universe. ESA Publications, Noordwijk, p. 497
Takahashi T. et al., 2007, PASJ, 59, 35
Takahashi T. et al., 2010, Proc. SPIE, 7732, 77320Z
Thompson D. J. et al., 1995, ApJS, 101, 259
Valinia A., Marshall F. E., 1998, ApJ, 505, 134
Zavlin V. E., Pavlov G. G., Shibanov Y. A., 1996, A&A, 315, 141

This paper has been typeset from a TEX/LATEX file prepared by the author.